## NOTATION

$d_b$ = bubble diameter, m
$C_a$ = concentration of reactant A, mol/m$^3$
$g$ = acceleration due to gravity, m/s$^2$
$H_e$ = height at which bubble is fully formed, m
$k_s$ = reaction rate constant from packed bed data, s$^{-1}$
$n_b$ = bubble frequency, Hz
$Q$ = volumetric gas flow rate into expanded dense phase, m$^3$/s
$Q_{or}$ = volumetric gas flow rate through orifice, m$^3$/s
$R$ = bubble radius, m
$r_A$ = rate of reaction of $A$, mol/m$^3$·s
$t_d$ = bubble formation time, s
$t_e$ = bubble equilibration time, s
$U_b$ = bubble rise velocity, m/s
$U_{mf}$ = minimum fluidization velocity, m/s
$V_b$ = visible bubble volume, m$^3$
$x$ = fraction of orifice flow forming a visible bubble
$\epsilon$ = dense-phase voidage
$\epsilon_{mf}$ = dense-phase voidage at minimum fluidization

### Subscripts

1 = as seen 10 cm above distributor
2 = as seen 25 cm above distributor
0 = entry condition
$d$ = dense phase


## ACKNOWLEDGMENTS

We are grateful to the following students who carried out this experimental work as part of a course on gas fluidization: David Allen, Iphigenia Antoniou, David Beiny, David Blackburn, John Carter, Paul Christoforou, Huw Davies, Paul Gates, Leslie Gower, Neil Gravestock, Adrian Hide, Peter Hughes, Lee Beng Han, Ian McDermott, Michael Pappenheim, David Sage, Paul Thomas, Leslie Vaughan, and Michael Welch.

*Manuscript received November 9, 1983; revision received March 6, and accepted March 22, 1984.*


*[This manuscript is dedicated to the memory of C. Y. Wen]*

# Distribution of Bubble Properties in a Gas-Liquid-Solid Fluidized Bed


The behavior of bubbles in a cocurrent gas-liquid-solid fluidized bed was investigated in a column of 76.2 mm ID in this study. The particles used were glass beads of 3 and 6 mm and a binary mixture of these particles. A novel dual electrical resistivity probe system was developed and utilized to obtain bubble properties including bubble size and rise velocity. The distributions of the bubble properties in the gas-liquid-solid fluidized bed were evaluated for three flow regimes: the dispersed bubble flow regime; the coalesced bubble flow regime; and the slug flow regime.



**AKINORI MATSUURA and LIANG-SHIH FAN**

Department of Chemical Engineering
The Ohio State University
Columbus, OH 43210


## SCOPE

Gas-liquid-solid fluidized beds have been fully developed and demonstrated in processing technology; as three-phase reactors, they have been employed in the H-oil process for hydrogenation and hydrodesulfurization of residual oil, the H-coal process for coal liquefaction, and the bio-oxidation process for waste water treatment.

A knowledge of hydrodynamics is of considerable importance in design and operation of a gas-liquid-solid fluidized bed. Among various hydrodynamic properties, bubble size and rise velocity and their distributions are of prime concern, as they are directly responsible for the behavior of other hydrodynamic properties such as liquid flow patterns, solids mixing, and gas-liquid interfacial area.

Very limited information is available in the literature regarding the in-bed bubble size or rise velocity distributions in the gas-liquid-solid fluidized bed. Page and Harrison (1972) used photographic techniques to examine the size distribution of bubbles leaving a gas-liquid-solid fluidized bed and found that the logarithmic cumulative distribution function varies linearly with bubble size. Using an impedance double-probe, Darton and Harrison (1974) reported that bubble size in a three-phase fluidized bed of 500 $\mu$m sand particles follows a log-normal distribution.

This study is directed toward a fundamental understanding of in-bed bubble properties including bubble size and bubble rise velocity in a gas-liquid-solid fluidized bed of large particles and their mixture. The bubble properties are distinguished for each of the three flow regimes; dispersed bubble flow regime; coalesced bubble flow regime; and slug flow regime.

## CONCLUSIONS AND SIGNIFICANCE

A novel dual electrical resistivity probe was developed to obtain the distribution of bubble rise velocity and size in a gas-liquid-solid fluidized bed containing large particles. The probe used possessed adequate strength to sustain the impact of solid particles, yet was small enough to allow bubbles of small size to be detected. The experiments were conducted in a circular plexiglas column of 76.2 mm ID. The particles used were 3 and 6 mm glass beads and a binary mixture of them. The behavior of bubble properties in each of the three flow regimes


Correspondence concerning this paper should be addressed to L. S. Fan.

was examined including dispersed bubble flow regime, coalesced bubble flow regime, and slug flow regime.

The bubble rise velocity depends strongly on the flow regime under which the system is operated. The bubble rise velocity in the slug flow regime exhibits the broadest distribution, followed by that in the coalesced bubble flow regime and the dispersed bubble flow regime. The bubble rise velocity distribution is practically insensitive to the particle size considered in this study.

The in-bed bubble size distribution in each of the three flow regimes is obtained from the directly measured chord length distribution and the probability of a bubble striking the probe over the projected area of the bubble. The bubble size distribution can be expressed in terms of a log-normal distribution. The mean bubble size can be related to the mean chord length by a linear equation. The mean bubble size obtained in the present study is bounded by two theoretical relationships for spherical and spheroidal bubbles, which can be obtained for the case of uniform sized bubbles. Also the experimentally obtained mean bubble size shows a specific trend of variation from the bound for a spherical bubble at a small mean chord length to the bound for a spheroidal bubble at a large mean chord length. The mean bubble size plotted against the bed expansion parameter, the ratio of expanded bed height to static bed height, shows clearly that the mean bubble size also depends strongly on flow regime. In the dispersed bubble flow regime, a small mean bubble size is observed and the mean bubble size increases only slightly with an increase in the bed expansion parameter. In the coalesced bubble flow regime and slug flow regime, a large mean bubble size is observed. The bubble size increases considerably with an increase in the bed expansion parameter for the coalesced bubble flow regime but increases moderately for the slug flow regime.

The variance of the bubble size distribution is proportional to the square of the mean bubble size for all types of particles and flow regimes considered. It is noted that a small mean bubble size is associated with a small variance, while a large mean bubble size is associated with a large variance. Additionally, a small variance in the bubble size distribution characterizes dispersed bubble flow, while a large variance characterizes coalesced bubble flow as well as slug flow. The bubble size distribution is practically insensitive to the variation in the particle properties considered in this study.

For comparison, $\bar{d}_v$, the mean bubble size based on the volume frequency of the bubbles, is defined by assuming a spherical bubble geometry. The value of $\bar{d}_v$ is in general larger than that of the mean bubble size based on the number frequency of the bubbles, $\bar{d}_n$. In particular, $\bar{d}_v$ is considerably higher than $\bar{d}_n$ in the slug flow regime due to the effect of the large volume of gas slugs.

## INTRODUCTION

Gas-liquid-solid fluidized bed operation is of considerable importance in chemical, petrochemical and biochemical processing. The performance of a gas-liquid-solid fluidized bed is dictated to a great extent by bubble behavior in the bed. A knowledge of bubble properties such as gas-phase holdup, bubble size and rise velocity, and their distribution is thus of prime concern in the fundamental understanding of a gas-liquid-solid fluidized bed.

Efforts have been made to obtain the bubble size in relation to the bed operating conditions in a single bubble system (Massimilla et al., 1961; Henriksen and Ostergaard, 1974; El-Temtamy and Epstein, 1980). Henriksen and Ostergaard (1974) found that the relationship between bubble size and bubble rise velocity can be represented by an equation similar to that obtained by Davies and Taylor (1950) for spherical cap bubbles. For a multibubble system, efforts have been made in experiments to obtain the bubble size and its axial variation in fluidized beds containing particles of diameter less than about 1 mm (Adlington and Thompson, 1965; Ostergaard, 1966; Rigby et al., 1970). Lee (1965) reported that, in a three-phase fluidized bed of 6-mm glass beads, the breakage of bubbles by the particles is such that bubble size decreases with an increase in bed height. Using an electroresistivity probe, Rigby et al. (1970) found that, for particle with sizes from 120 to 775 $\mu$m, bubbles coalesce as they move up the bed. They also reported that the mean bubble size increases with a decrease in liquid flow rate, increases with an increase in gas flow rate, and increases with increasing axial distance. Rigby et al. (1970) also indicated that the distribution of the bubble size becomes wider as the axial distance increases or as the liquid flow rate decreases. Bruce and Revel-Chion (1970) examined the size of bubbles leaving a three-phase fluidized bed of large particles ranging from 2 mm to 8 mm and found that bubble size decreases with increasing particle size up to 6 mm and then increases with increasing particle size beyond 6 mm. Bruce and Revel-Chion (1974) indicated that for 6 and 8 mm particles, the bubble size decreases, reaches a minimum at a liquid velocity of around 13.2 cm/s, and then increases with an increase in liquid velocity. Furthermore, they indicated that the bubble size for 2 mm particles is virtually independent of gas velocity, while for a bed of 6 mm particles, the bubble size increases linearly with increasing gas velocity.

Page and Harrison (1972) examined the size distribution of bubbles leaving a three-phase fluidized bed of 500 $\mu$m particles with the aid of photographic techniques. They found that the logarithmic cumulative distribution function varies linearly with bubble size. Darton and Harrison (1974) reported that bubble size determined using an impedance probe in a three-phase fluidized bed of 500–600 $\mu$m sand particles follows a log-normal distribution, with a variance which increases with an increase in gas flow rate.

In practical application of a gas-liquid-solid fluidized bed, a size and/or density distribution of solid particles in the bed is commonly encountred. Vary little information, however, is available in the literature regarding the fundamental characteristics of the three-phase fluidized bed with mixed size and/or density particles. Fan et al. (1984) investigated solids mixing in cocurrent three-phase fluidized beds containing a binary mixture of glass beads with diameter ratios of 1.33 (3 and 4 mm particles) and 2.00 (3 and 6 mm particles). They noted that there exists a strong correlation between the solids mixing map and the flow regime map.

In this study, a dual electrical resistivity probe was developed which allows a study of in-bed properties of bubbles in a three-phase fluidized bed of large particles. the particles under consideration include glass beads of 3 and 6 mm and a binary mixture of these particles. The fundamental behavior of bubbles are examined for three different flow regimes: the dispersed bubble flow regime; the coalesced bubble flow regime; and the slug flow regime.

## EXPERIMENTAL

A schematic diagram of the experimental apparatus is shown in Figure 1. The vertical plexiglas column has the dimensions of 76.2 mm ID with a height of 2.73 m. The column consists of three sections: the gas-liquid distributor section; the test section with a height of 1.38 m; and the gas-liquid disengagement section. The gas-liquid distributor, which is located at the bottom of the test section, is designed in such a manner that uniform distributions of liquid and gas can be maintained in the column. Details of the gas-liquid distributor are given by Fan et al. (1982). Water and air are used as the liquid and gas phases in the experiments. The gas-liquid flow is cocurrent and upward. The particles used are 3 and 6 mm glass beads (densities are 2,590 and 2,520 kg/m$^3$, respectively) and a binary mixture of them with a weight ratio of 1 to 1. Note that the static bed height for all runs is set at about 26 cm.

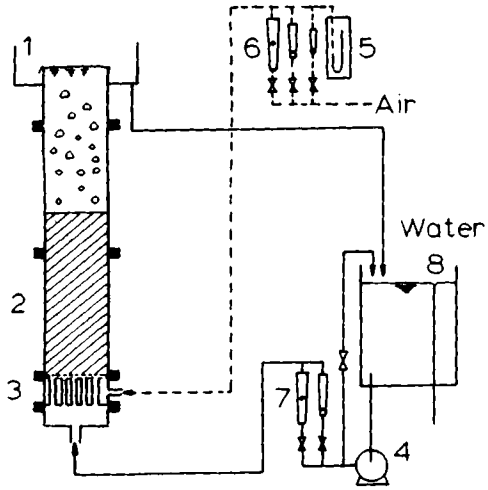


1 Gas-Liquid Disengagement Section
2 Test Section
3 Gas-Liquid Distributor Section
4 Liquid Pump
5 Pressure Gauge
6, 7 Rotameter
8 Liquid Reservoir

**Figure 1. Schematic diagram of the experimental apparatus.**

A novel dual electrical resistivity probe system was developed and utilized to measure local bubble size, rise velocity, and freuency of the bubble phase in the gas-liquid-solid fluidized bed. The probe, to which 3 V DC is applied, detects the difference in conductivity of gas and liquid. The analog signals obtained from each probe circuit are reformed to produce signal of square wave rorm. A pair of signals which correspond to a bubble striking the dual probe is selected automatically in the logic circuit. An apparent lag time corresponding to the passage of the bubble between the two tips of the dual probe and the duration of the time in which the bubble passes through the probe tip are measured and printed out on a digital printer. Data processing is conducted in real time.

### Probe System

The setup of the resistivity probe in the experimental system is shown in Figure 2. The placement of the probe can be altered during the fluidized bed operation by moving the support tubing with the aid of a calibrated moving bar.

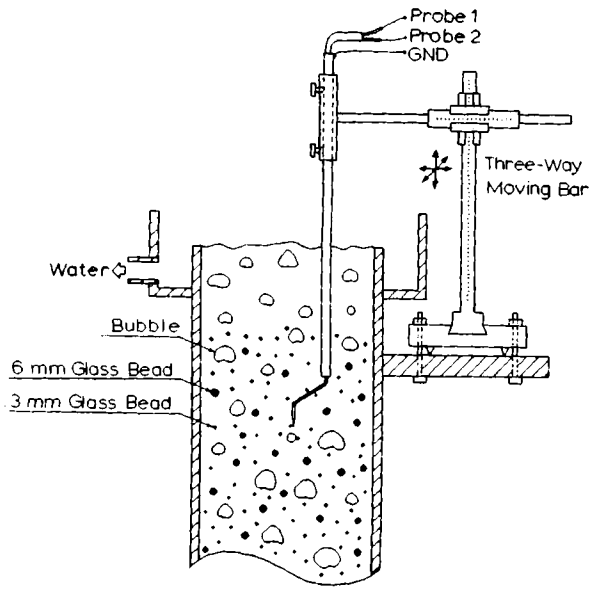


**Figure 2. Schematic diagram of the probe setup in the three-phase fluidized bed with a binary mixture of particles.**

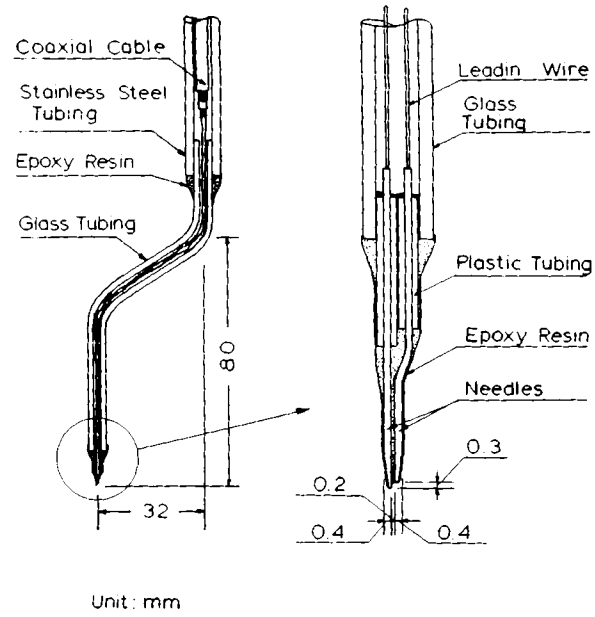


**Figure 3. Details of the dual electrical resistivity probe.**

The probe used in the gas-liquid-solid fluidized bed of large particles is designed in such a manner that it possesses adequate strength to sustain the impact of the solid particles and yet is small enough to allow tiny bubbles to be detected. Figure 3 shows details of the probe design. The dual electrical resistivity probe consists of two 0.4 mm diameter stainless steel syringe needles coated with epoxy resin. The vertical distance between the tips of the two needles is 0.3 mm. The tips of the needles, which are exposed to the experimental system, have a diameter of 0.2 mm each. The probe is supported by glass tubing and by stainless steel tubing which serves as the positive electrode. The shape of the support tubing is designed such that minimum flow disruption due to the presence of the probe in the bed is maintained.

### Signal Processing Circuit and Signal Acquisition

Figure 4 depicts the signal flow in the signal processing system. The system consists of amplifiers, signal reformers (comparators), a clock pulse generator, a logical processor, digital counters, a digital printer, an interface to a digital printer, and a power supply. An oscilloscope is also used to monitor the amplified signals.

The analog signals from the probe are amplified such that high-level signals, which correspond to liquid contact of the probe, are 5 V. Low-level signals or gas contact remain near zero. In the wave reform section, they are compared to a threshold signal intensity set at 80% of the high level of the amplified signal intensity. Note that this threshold level is identical to that used by Rigby et al. (1970) for an impedance double probe. All signal intensities above the threshold value signify the conductive liquid phase, and all signal intensities below the threshold value signify the nonconductive gas phase.

The relationship between reformed probe signals and bubble dwell and lag time is shown in Figure 5. The dwell time, $\tau$, of a bubble represents the duration of time in which the bubble passes through the probe, and the apparent lag time, $\Delta t$, represents the time interval between leading edges of a pair of signals corresponding to the passage of the bubble. Probe 1, or the upstream probe, and probe 2, or the downstream probe, are denoted by subscripts 1 and 2, respectively. To match a pair of signals due to the passage of a single bubble through the dual probe, the leading (negative going) edge of signal 1 at time $t_1$ is chosen as a trigger. This is followed by the trailing (positive going) edges at $t_3$ of signal 1, and the leading and trailing edges at $t_2$ and $t_4$, respectively, of signal 2. In the signal pair selection section of the logic circuit, these four edges create three signals which represent the time intervals between $t_1$ and $t_3$, or $\tau_1$, $t_2$ and $t_4$, or $\tau_2$, and $t_1$ and $t_2$ or $\Delta t$. The time intervals $\tau_1$, $\tau_2$, and $\Delta t$ are measured with the aid of clock pulses and gated digital counters.

The average residence time of a bubble traveling between the two tips of the probe, $\Delta\tau$, can be expressed by

$$\Delta\tau = (t_2 - t_1) + \frac{1}{2}(\tau_2 - \tau_1) = \Delta t + \frac{1}{2}(\tau_2 - \tau_1) \qquad (1)$$

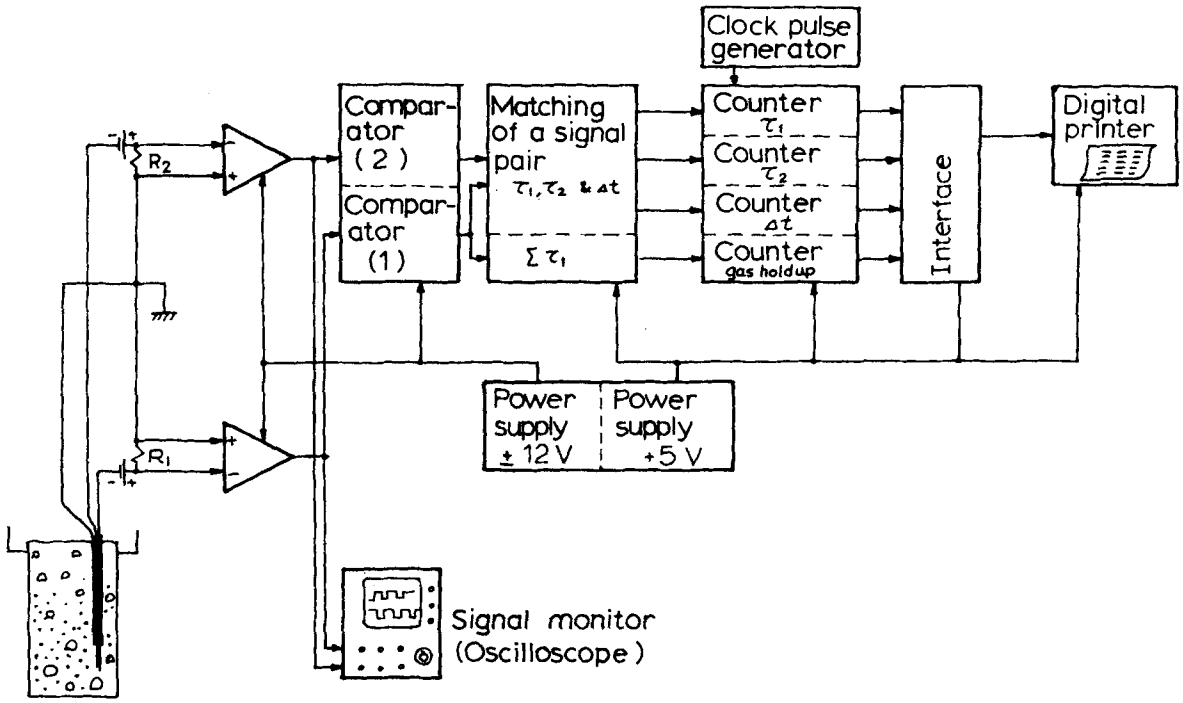


**Figure 4. Signal flow diagram for the probe measuring system.**

where $t$ is the real time. The bubble rise velocity, $u_b$, and chord length, $l_b$, can be calculated by the following equations:

$$u_b = L_p/\Delta\tau \tag{2}$$

$$l_b = \bar{\tau} u_b$$

$$= (\tau_1 + \tau_2)L_p/2\Delta\tau \tag{3}$$

where $L_p$ is the vertical distance between the two tips of the probe. The average bubble velocity can be calculated by (Ueyama et al., 1980):

$$\bar{u}_b = \frac{1}{n}\sum_{i=1}^{n} u_{b_i} \tag{4}$$

An error may result from the fact that a bubble detected by probe 2 is not always preceeded by a bubble detected by probe 1. For instance, a bubble penetrated by probe 1 may be deflected and not strike probe 2. In another case, a bubble pierced by probe 1 may not be deflected, but before it can reach probe 2 another bubble that missed probe 1 touches probe 2. In addition to the cases mentioned above, a slight deflection of a bubble striking probe 1 may result in a different dwell time of the bubble on probe 2. To accept a signal pair received when a bubble passes through both probes requires several conditions be satisfied. This so-called "matching of a signal pair" is made automatically in the logic circuit in which the following constraints are placed:

1) The signal for probe 1 is used as a trigger signal.
2) It requires $t_1 < t_2$.
3) It requires $t_1 + \tau_1 < t_2 + \tau_2$.
4) It requires $0.9 < \dfrac{\tau_1}{0.5(\tau_1 + \tau_2)} < 1.1$.

A signal pair which does not satisfy all the constraints described above is ignored. Note that about 50% or less of the signal pairs detected by the probe were ignored for a typical bubble property measurement for the dispersed bubble flow regime, whereas about 65% or less of those for the coalesced bubble flow regime and 80% or less of those for the slug flow regime were ignored.

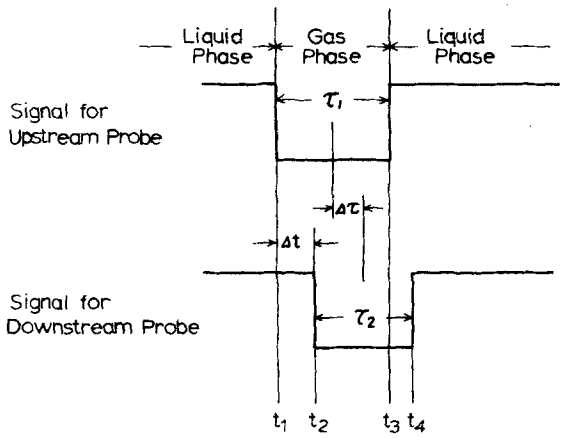


**Figure 5. Relationship between probe signals and bubble dwell and lag times.**

### Chord Length Distribution vs. Bubble Size Distribution

The bubble chord length distribution, $z(l_b)$, obtained directly from the probe is related to $p(d,l_b)$, the probability of a bubble of size $d$ striking the probe over the projected area of the bubble, and $r(d)$, the actual bubble size distribution at a specific location, according to

$$z(l_b) = \int_{l_b}^{\infty} p(d,l_b) r(d) dd. \tag{5}$$

Note that the size of a bubble refers to the vertical length of a chord passing through the center of the bubble. Tsutsui and Miyauchi (1980) have indicated that for a spherical bubble or a nonspherical bubble, which can be approximated by a pair of concentric spheroids, $p(d,l_b)$ can be expressed by:

$$p(d,l_b) = 2l_b/d^2, \quad \text{for } l_b \leqq d \tag{6}$$

In reality the upperbound of integration on the righthand side of Eq. 5 is finite. Thus, Eq. 5 is rewritten in dimensionless form as

$$Z(\lambda) = \int_{\lambda}^{\xi_m} \frac{2\lambda}{\xi^2} R(\xi) d\xi \tag{7}$$

where $\xi_m$ is the maximum value of $\xi$.

The definite integral on the righthand side of Eq. 7 can be closely approximated by any of several numerical integration formulas, and replaced by an integration formula with $m$ points of subdivision of the $\lambda$- and $\xi$-axes and the weight coefficients $w_i$, $i = 1, \ldots, m$, whose values depend on the type of numerical integration formula used. One can obtain $m$ linear algebraic equations for the $m$ unknowns, $R(\xi_1), \ldots, R(\xi_m)$. Using a simple quadrature formula with specified nodes Eq. 7 can be expressed by

$$\begin{bmatrix} Z(\lambda_1) \\ Z(\lambda_2) \\ \vdots \\ Z(\lambda_{m-1}) \\ Z(\lambda_m) \end{bmatrix} = \begin{bmatrix} w_1 p(\xi_1,\lambda_1) w_2 p(\xi_2,\lambda_1) \cdots\cdots & & w_m p(\xi_m,\lambda_1) \\ & w_2 p(\xi_2,\lambda_2) \cdots\cdots & w_m p(\xi_m,\lambda_2) \\ & \vdots & \\ & w_{m-1} p(\xi_{m-1},\lambda_{m-1}) & w_m p(\xi_m,\lambda_{m-1}) \\ & & w_m p(\xi_m,\lambda_m) \end{bmatrix} \begin{bmatrix} R(\xi_1) \\ R(\xi_2) \\ \vdots \\ R(\xi_{m-1}) \\ R(\xi_m) \end{bmatrix} \Delta\xi \tag{8}$$

In inversion matrix form, Eq. 8 becomes

$$\begin{bmatrix} R(\xi_1) \\ R(\xi_2) \\ \vdots \\ R(\xi_m) \end{bmatrix} = \begin{bmatrix} w_1 p(\xi_1,\lambda_1)\, w_2 p(\xi_2,\lambda_1) \cdots\cdots & w_m p(\xi_m,\lambda_1) \\ & w_2 p(\xi_2,\lambda_2) \cdots\cdots & w_m p(\xi_m,\lambda_2) \\ & \vdots & \\ & & w_m p(\xi_m,\lambda_m) \end{bmatrix}^{-1} \begin{bmatrix} Z(\lambda_1) \\ Z(\lambda_2) \\ \vdots \\ Z(\lambda_m) \end{bmatrix} \frac{1}{\Delta\xi} \tag{9}$$

Thus $R(\xi)$ can be obtained directly from the inversion of the diagonal matrix and $Z(\lambda)$ as given in Eq. 9. Note that $w_i$, $i = 1, \ldots, m$ is taken as 1 in the present numerical computation, since the subdivision of the $\lambda$- and $\xi$-axes for numerical integration is chosen to be small as compared with the mean of the bubble size distribution (Matsuura et al., 1976).

## RESULTS AND DISCUSSION

There is a distinct difference in bubble size behavior between the gas-solid fluidized bed and gas-liquid-solid fluidized bed. In general, in the gas-solid fluidized bed the average bubble size increases with axial distance. The bubble size distribution at a given axial distance exhibits a small variance. Compared to the gas-solid fluidized bed, the bubble size behavior in the gas-liquid-solid fluidized bed is much more complicated. There is a wide range of distribution of bubble sizes at a given axial distance in the gas-liquid-solid fluidized bed. The bubble size distribution varies considerably with axial distance. Furthermore, as will be discussed later, the bubble size distribution also depends on the flow regime.

For any bubble property distribution reported in this study, at a given fluidization condition, about 500 data points are taken.

The minimum detectable bubble size using the present probe is predicted to be approximately 0.1 cm, based on the following empirical correlation proposed by Buchholz et al. (1981) for the minimum bubble size detectable by a probe:

$$d_{\min} = 4\Delta d_h + d_r + a \tag{10}$$

where

$\Delta d_h$ = horizontal distance between the centers of two needles
$d_r$ = needle diameter
$a$ = insulation constant

### Probe Method vs. Photographic Method

It should be noted that the shape of the support tubing for the probe is designed in such a manner that minimum flow disruption due to the presence of the probe is maintained, as described earlier. The probe's effect on bubble properties is examined visually using a separate bubble column with a rectangular cross-section. The dimensions of the column are 38.0 mm × 76.2 mm × 1,000 mm. Bubbles are injected through a tube injector located at the center of the bottom plate into the quiescent liquid column. The sizes of two single tube injectors are 0.63 and 4.0 mm ID. The small-size injector is used to generate small bubbles while the large-size injector is used to generate large bubbles. The probe is positioned a short distance above the injector to allow effective interception of small bubbles. The probe is positioned a moderately long distance (about 60 cm) above the injector for measurement of large bubble sizes. An audio-video camera, a recorder, T.V., and a stroboscope with a flash rate of 36 Hz constitute the photographic system.

Bubbles are generated at a certain time interval. When a bubble strikes the probe, the audio-video recorder registers the sound generated by the printer in the probe system. The sound is used to permit identification of the particular bubble shown on the T.V. screen. In this way the bubble property measurements of the photographic and probe methods are synchronized. The replayed audio-video images are used to visually measure the bubble properties prior to the bubbles striking the probe, i.e., immediately below the probe. Figures 6 and 7 show the comparison of bubble rise velocities and chord lengths obtained by these two methods. It is seen that the data points obtained by the present probe device are within ±20% of those obtained photographically over a wide range of bubble chord lengths from 1 to 40 mm. It is evident, however, that for a majority of the bubble rise velocity and chord length data, the present probe device gives rise to slightly lower values than the photographic measurement. This discrepancy may

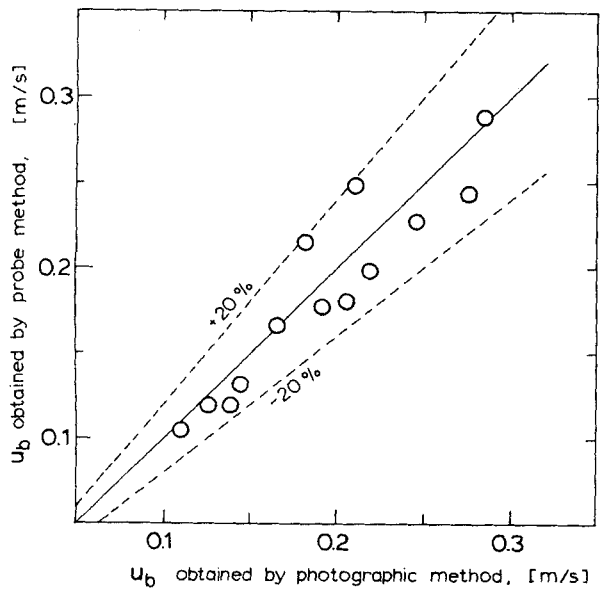


Figure 6. Comparison of bubble rise velocity obtained by probe method and photographic method.

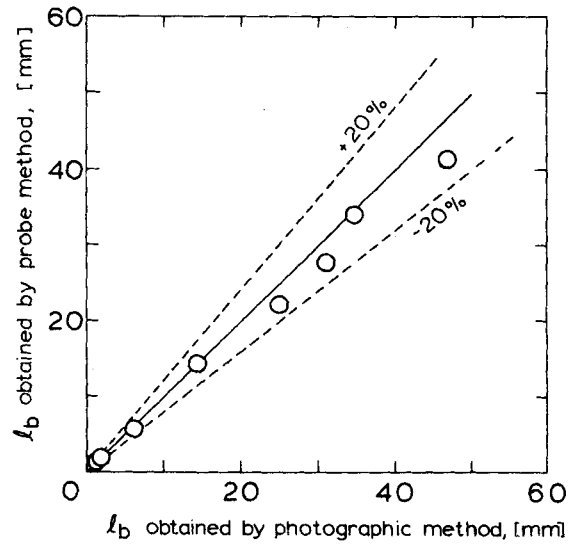


Figure 7. Comparison of chord length obtained by probe method and photographic method.

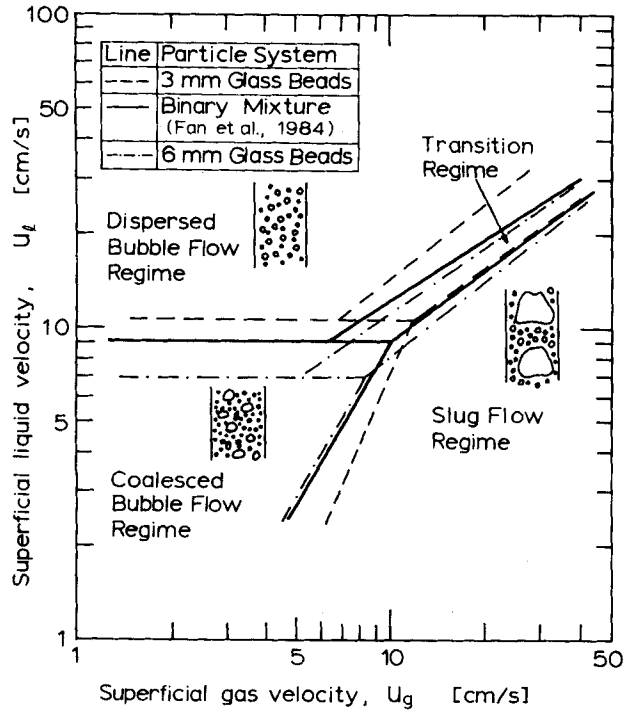


**Figure 8. Flow regime map for 3 and 6 mm glass beads and a binary mixture of these particles with a weight ratio of 1 to 1.**

be due to the fact that photographic method measures projected properties of the bubble whereas the probe method measures *in situ* properties. For example, surface identations common in large bubble geometries are more accurately detected by the probe method, and thus their effect on bubble properties more accurately reflected.

During the photographic measurements, tiny hydrogen bubbles are periodically observed at the tip of the probe. It is noted that these bubbles are quickly detached from the probe tip after their formation due to the vigorous motion of liquid surrounding the probe. No hydrogen bubble effect on the bubble properties is evident in the video analysis.

### Flow Regime

Hydrodynamic characteristics including bed expansion, solids mixing, and flow regime for a three-phase fluidized bed containing a binary mixture of 3 and 6 mm glass beads has recently been explored by Fan et al. (1984). Figure 8 shows the flow regime map expressed in terms of liquid velocity vs. gas veocity for 3 and 6 mm glass beads and for the binary mixture. Clearly, three flow regimes can be distinguished in the system, namely, the dispersed bubble flow regime, coalesced bubble flow regime, and slug flow regime. Note that dispersed bubble flow represents the flow pattern under which bubbles of fairly uniform size are observed in the gas-liquid-solid fluidized bed. Slug flow represents the flow pattern under which large slugs, whose vertical length is greater than or close to the column diameter, are observed from the outside of the column. Coalesced bubble flow indicates that spherical cap or spheroidal bubbles of various sizes are observed in the three-phase fluidized bed. Based on the flow regime map, gas and liquid velocities are chosen in this study to reflect the flow regime effect on bubble behavior for 3 and 6 mm glass beads and a binary mixture of particles. For comparison, bubble properties are evaluated at the center of the bed and two thirds of the expanded bed height away from the distributor for various fluidization conditions.

### Bubble Rise Velocity

Figures 9a, b, and c show the bubble rise velocity distribution for a binary mixture of particles in the dispersed bubble flow regime, slug flow regime, and coalesced bubble flow regime. Note that the bubble rise velocity, $u_b$, represents an absolute velocity with respect to the column wall, and that the velocity distribution, $Q(u_b)$, given here is based on the number frequency of the bubble rise velocities. In the dispersed bubble flow regime, the bubble rise velocity is narrowly distributed. The mean bubble rise velocity for a binary mixture of particles is 0.548 m/s. The mean bubble rise velocities for 3 and 6 mm glass beads are 0.528 and 0.529 m/s, re-

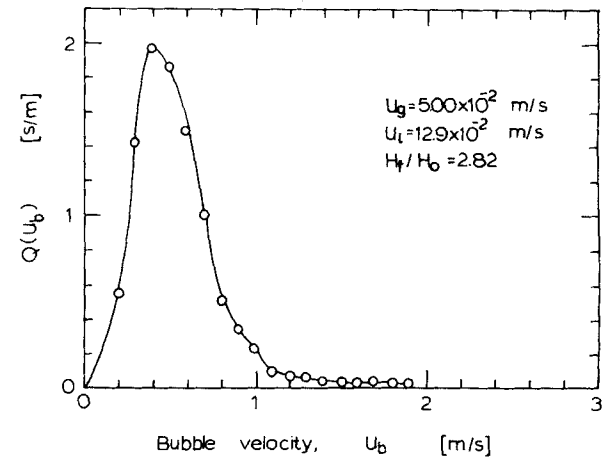


**Figure 9a. Bubble rise velocity distribution for a binary mixture of particles in the dispersed bubble regime.**

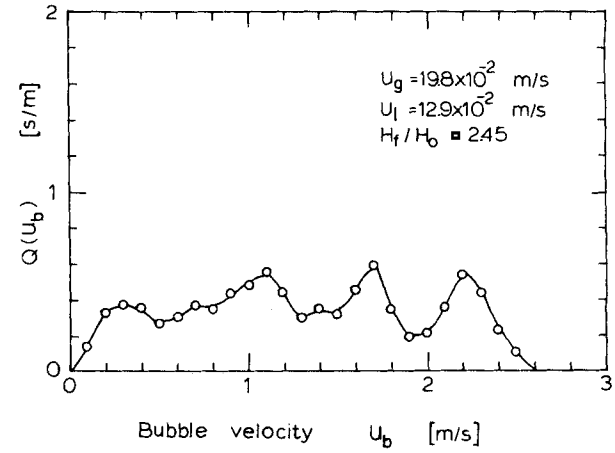


**Figure 9b. Bubble rise velocity distribution for a binary mixture of particles in the slug flow regime.**

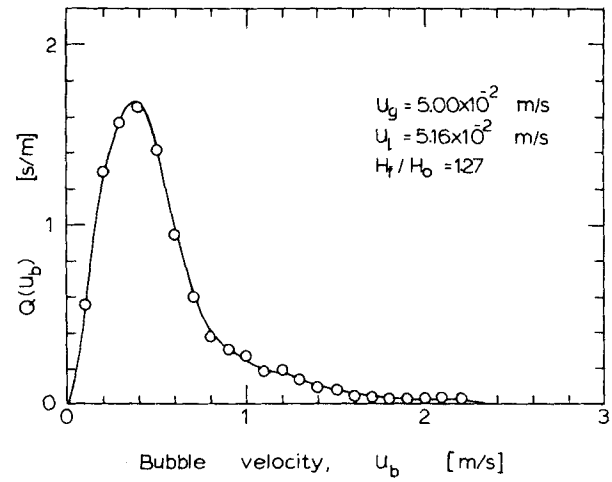


**Figure 9c. Bubble rise velocity distribution for a binary mixture of particles in the coalesced bubble flow regime.**

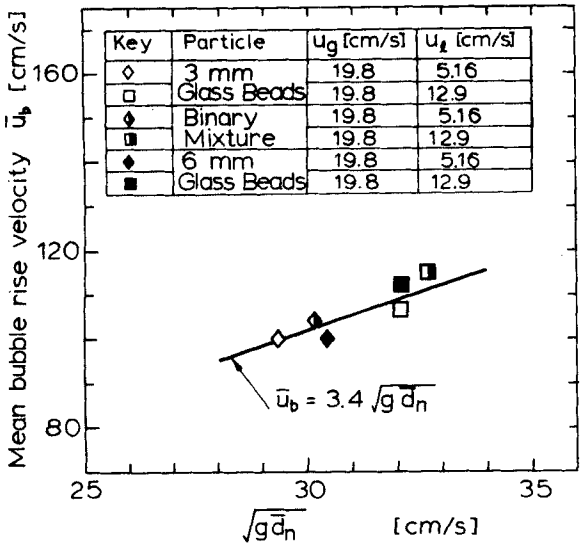


**Figure 10. Relationship between mean bubble rise velocity and mean bubble size in the slug flow regime.**

spectively. It can be stated that in the dispersed bubble flow regime the variation of the mean and distribution of the bubble rise velocities is insensitive to the particle size considered in this study.

In the slug flow regime the bubble rise velocity distribution exhibits multimodal behavior. The bubble rise velocity is distributed over a considerably wide range with the largest slug velocity observed as 2.5 m/s. The mean bubble rise velocity in the slug flow regime for the three particle systems considered varies in the range from 1.07 to 1.15 m/s. Figure 10 shows that the mean bubble rise velocity in the slug flow regime follows closely the following equation

$$\bar{u}_b = 3.4\sqrt{g\bar{d}_n} \tag{11}$$

where

$$\bar{d}_n = \text{mean bubble size}$$

It is also noted that in the slug flow regime the small bubbles behind the large slug travel at a much higher velocity than small bubbles of the same diameter in the dispersed bubble flow regime.

In the coalesced bubble flow regime, the bubble rise velocity distribution is similar to that in the dispersed bubble flow regime except that the tail of the distribution in the coalesced bubble flow regime extends to much higher bubble rise velocities. It is noted that the mean bubble rise velocity in the coalesced bubble flow regime is slightly smaller than that in the dispersed bubble flow regime.

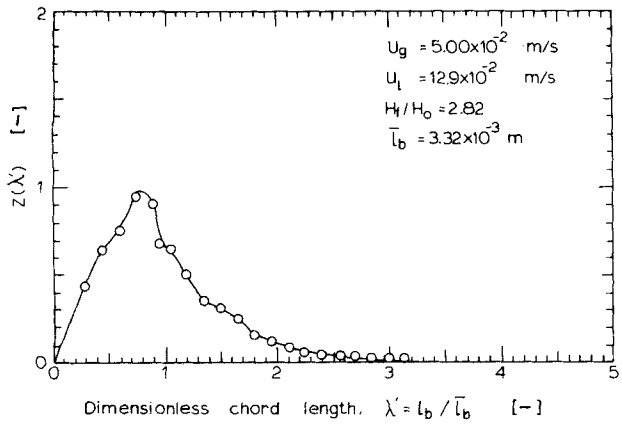


**Figure 11. Chord length distribution for a binary mixture of particles in the dispersed bubble flow regime.**

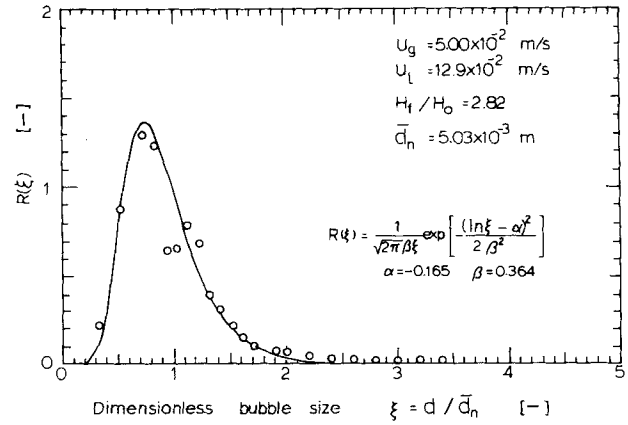


**Figure 12a. Bubble size distribution for a binary mixture of particles in the dispersed bubble flow regime.**

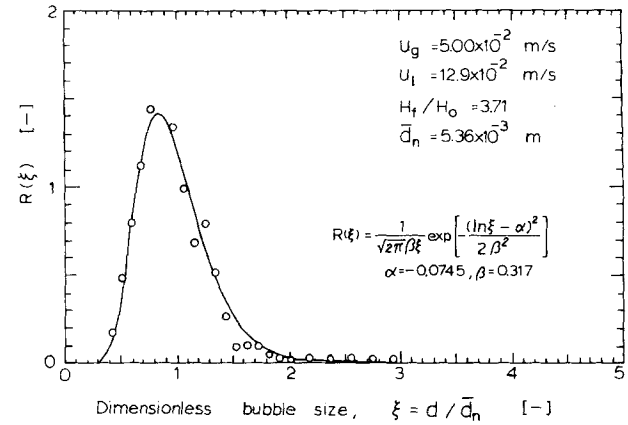


**Figure 12b. Bubble size distribution for 3mm glass beads in the dispersed bubble flow regime.**

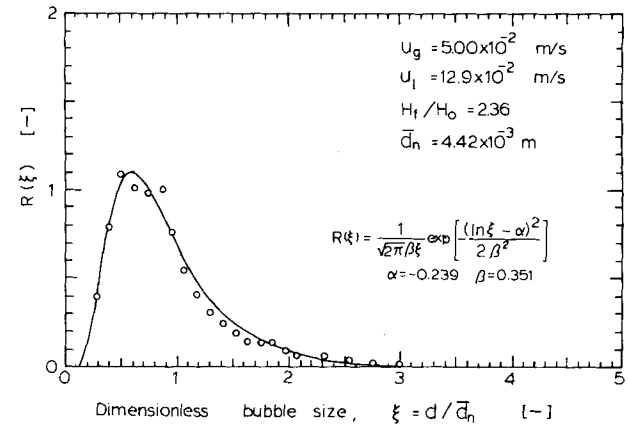


**Figure 12c. Bubble size distribution for 6mm glass beads in the dispersed bubble flow regime.**

Evidently, the flow regime has a strong effect on the bubble rise velocity distribution while little effect is observed of the particle property on the distribution.

### Chord Length and Bubble Size Distribution

Figure 11 shows the chord length distribution for the binary mixture of particles in the dispersed bubble flow regime. The mean chord length in this distribution is 0.332 cm. It is seen that the distribution extends over a wide range of dimensionless chord lengths (up to 3.2). The bubble size distribution in the dispersed bubble flow regime for the binary mixture and 3 and 6 mm glass beads are shown in Figures 12a, b, and c. Note that the bubble size

TABLE 1. VALUES OF MEAN CHORD LENGTH, MEAN BUBBLE SIZE AND LOG-NORMAL DISTRIBUTION PARAMETERS OBTAINED IN THIS STUDY

| Flow Regime | Particle System | $\bar{l}_b$ [mm] | $\bar{d}_n$ [mm] | $\alpha^{(*)}$ | $\beta^{(*)}$ | $\sigma^{2(**)}$ | $\bar{d}_v^{(***)}$ [mm] | $H_f/H_o$ |
|---|---|---|---|---|---|---|---|---|
| Dispersed Bubble | | | | | | | | |
| Flow Regime | Binary Mixture | 3.32 | 5.03 | −0.165 | 0.364 | 0.117 | 11.16 | 2.82 |
| $u_g$ = 5.00 cm/s | 3 mm Glass Beads | 3.80 | 5.36 | −0.0745 | 0.317 | 0.101 | 8.97 | 3.71 |
| $u_l$ = 12.9 cm/s | 6 mm Glass Beads | 3.05 | 4.42 | −0.239 | 0.351 | 0.0921 | 10.90 | 2.36 |
| Slug Flow Regime | Binary Mixture | 8.37 | 10.94 | −0.348 | 0.650 | 0.401 | 54.17 | 2.45 |
| $u_g$= 19.8 cm/s | 3 mm Glass Beads | 8.11 | 10.46 | −0.615 | 0.710 | 0.317 | 50.45 | 2.47 |
| $u_l$ = 12.9 cm/s | 6 mm Glass Beads | 7.28 | 10.51 | −0.524 | 0.721 | 0.402 | 65.98 | 2.45 |
| Slug Flow Regime | Binary Mixture | 6.96 | 9.22 | −0.646 | 0.750 | 0.364 | 37.68 | 1.45 |
| $u_g$ = 19.8 cm/s | 3 mm Glass Beads | 6.55 | 9.06 | −0.569 | 0.660 | 0.270 | 44.20 | 1.44 |
| $u_l$ = 5.16 cm/s | 6 mm Glass Beads | 6.48 | 9.46 | −0.584 | 0.689 | 0.303 | 62.21 | 1.45 |
| Coalesced Bubble | | | | | | | | |
| Flow Regime | Binary Mixture | 8.08 | 8.74 | −0.326 | 0.700 | 0.538 | 29.39 | 1.27 |
| $u_g$ = 5.00 cm/s | 3 mm Glass Beads | 6.16 | 8.92 | −0.297 | 0.677 | 0.508 | 19.92 | 1.28 |
| $u_l$ = 5.16 cm/s | 6 mm Glass Beads | 4.87 | 7.28 | −0.380 | 0.650 | 0.375 | 29.34 | 1.09 |

* $\alpha$ and $\beta$ are a natural log of a scale parameter and a shape parameter of log-normal distribution, respectively, in Eq. 12.
** $\sigma^2$ is the variance of log-normal distribution, given in Eq. 14.
*** $\bar{d}_v$ is the mean bubble size based on volume frequency of bubbles.

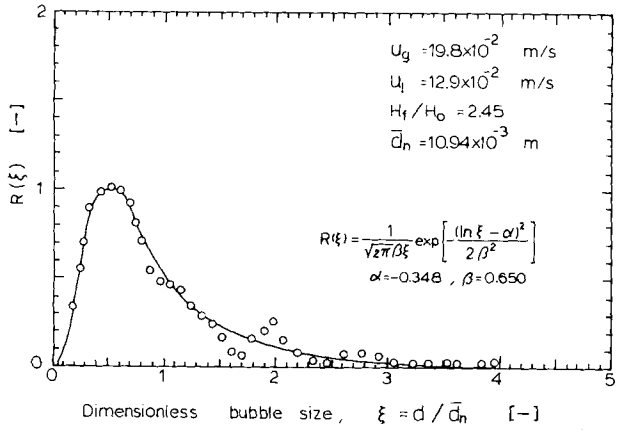


Figure 13. Bubble size distribution for a binary mixture of particles in the slug flow regime.

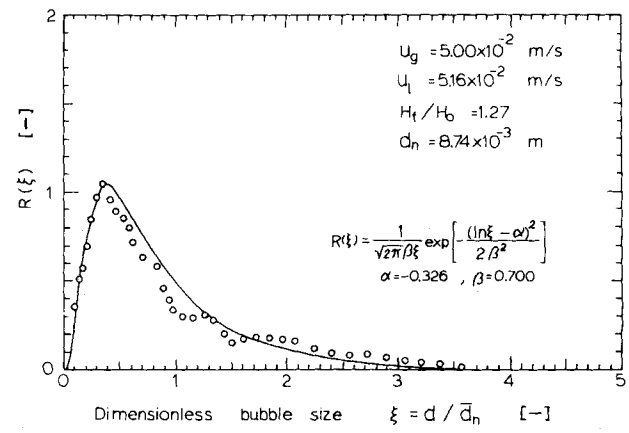


Figure 14. Bubble size distribution for a binary mixture of particles in the coalesced bubble flow regime.

distribution is obtained directly from the measured chord distribution as given by Eq. 5. The bubble size distributions for three particle systems studied are similar except that the distributions have small variations in the mean bubble sizes and the variances of the distributions. Furthermore, all of the distributions are shown to follow the log-normal distribution given below:

$$R(\xi) = \frac{1}{\sqrt{2\pi}\xi\beta} \exp\left[-\frac{(\ln\xi - \alpha)^2}{2\beta^2}\right] \tag{12}$$

where $\alpha$ and $\beta$ are a natural log of a scale parameter and a shape parameter of the log-normal distribution, respectively. The parameters, $\alpha$ and $\beta$ for the log-normal distribution are obtained by minimizing the standard deviation between the experimental observation and log-normal distribution prediction based on the Marquardt method (Kuestler and Mize, 1973). The mean, $\mu$, and variance, $\sigma^2$, of the log-normal distribution can be given as

$$\mu = \exp(\alpha + \beta^2/2) \tag{13}$$

$$\sigma^2 = \exp(2\alpha + \beta^2)\{\exp(\beta^2) - 1\} \tag{14}$$

The calculated values of $\sigma^2$ based on Eq. 14 for various particle systems are given in Table 1. Also shown in Table 1 are the values for $\bar{l}_b$, $\bar{d}$, $\alpha$, $\beta$, variance, $\sigma^2$, and bed expansion parameter, $H_f/H_0$, for all the systems considered. It is noted that the calculated mean value of the distribution based on Eq. 13 is in agreement with that directly obtained from the experimental data.

Figures 13 and 14 show the bubble size distributions for the binary mixture of particles in the slug flow regime and coalesced bubble flow regime, respectively. Again, it is found that these distributions can be expressed in terms of log-normal distributions. The distributions are seen to be similar except that the slug flow has a large mean bubble size compared to the coalesced bubble flow.

### Correlation

Figure 15 shows the relationship between the mean bubble size and the mean chord length for various types of particles and flow regimes. It is seen that the mean bubble size can be correlated with the mean chord length by the following equation:

$$\bar{d}_n = 1.34\,\bar{l}_b + 0.42 \tag{15}$$

Also shown in Figure 15 is the plot of the mean bubble size vs. mean chord length for spherical and spheroidal bubbles, which can be described respectively by the following theoretical relationships. For the case of uniform sized spherical bubbles (Ueyama and Miyauchi, 1976):

$$\bar{d}_n = 1.5\,\bar{l}_b \tag{16}$$

And for a pair of spheroidal bubbles of uniform size;

$$\bar{d}_n = 1.33\,\bar{l}_b \tag{17}$$

It is interesting to note that the data points in Figure 15 are bounded by Eqs. 16 and 17 with a specific trend of variation from the bound of Eq. 16 at a small mean chord length to the bound of Eq. 17 at a large mean chord length. The correlation of Eq. 15 signifies that bubbles with a small mean chord length are more spherical in shape

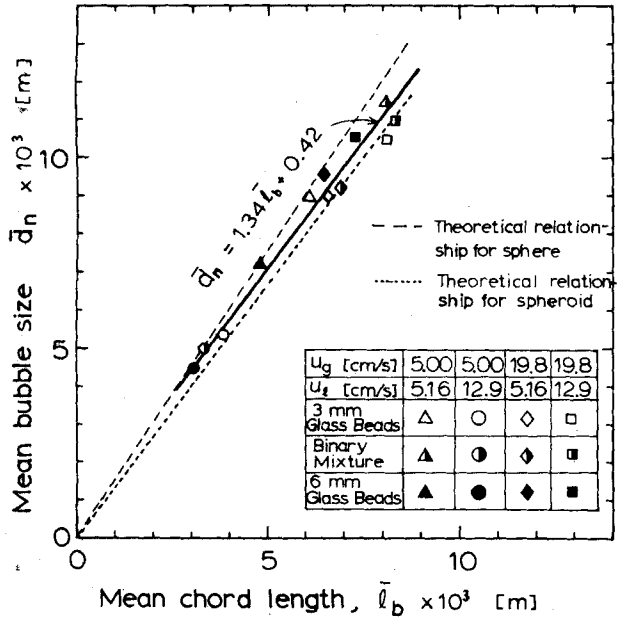


**Figure 15. Relationship between mean bubble diameter and mean chord length for various types of particles and flow regimes.**

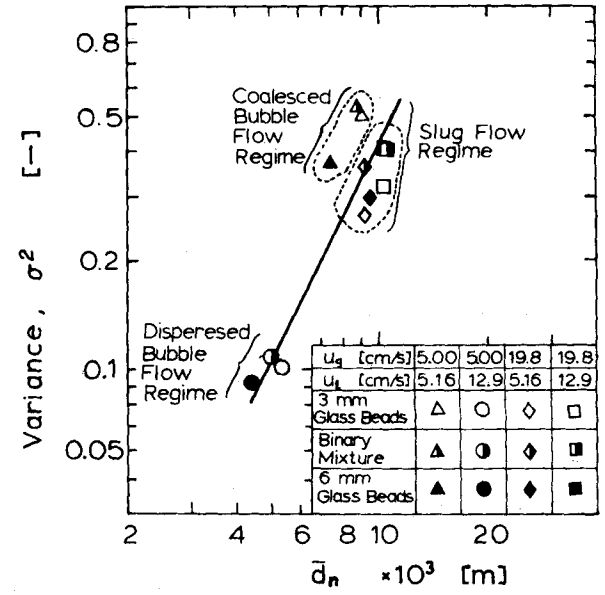


**Figure 17. Relationship between variance and mean of bubble size distribution for various types of particles and flow regimes.**

whereas bubbles with a large mean chord length are more spheroidal in shape. The linear relationship between mean chord length and Sauter mean bubble size has also been reported in the literature for gas-liquid systems (Ueyama et al., 1980) and for gas-liquid-solid slurry systems (Smith et al., 1983).

Figure 16 shows the relationship between the mean bubble size and the bed expansion parameter for the various flow regimes considered in this study. The bed expansion parameter, which is expressed as $H_f/H_0$, where $H_f$ is expanded bed height and $H_0$ is static bed height, represents the operating characteristics of various fluidization conditions considered in this study. The bed expansion parameter also reflects the holdup of solid particles in the bed. It is seen in Figure 16 that, in the dispersed bubble flow regime, a small mean bubble size is observed and the mean bubble size increases only slightly with an increase in the bed expansion parameter. In the coalesced bubble flow regime, a large mean bubble size is observed. The mean bubble size increases considerably with an increase in the bed expansion parameter for the coalesced bubble flow regime but increases moderately for the slug flow regime. Evidently, the flow regime has a strong effect on the mean bubble size. Moreover, the mean bubble size is practically insensitive to the particle properties considered in this study. For the dispersed bubble flow regime and coalesced bubble flow regime, the mean bubble size for 6 mm glass beads is the smallest, followed by that for the binary mixture and 3 mm glass beads, for which the mean bubble sizes are very close.

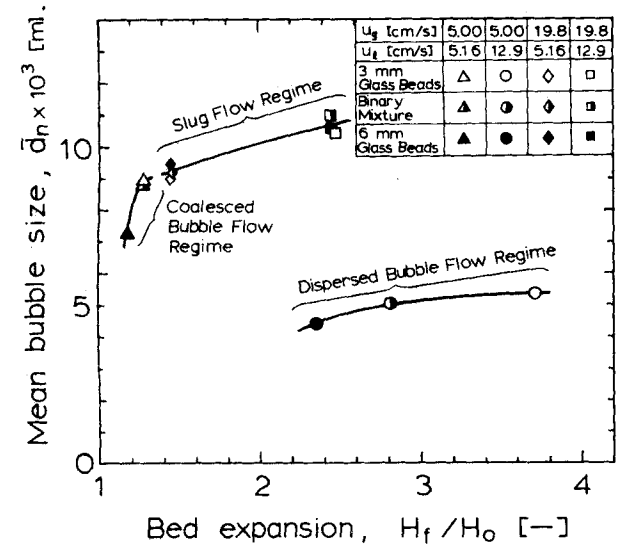


**Figure 16. Relationship between mean bubble size and bed expansion parameter.**

Figure 17 shows the relationship between the variance and mean of the bubble size distribution for various types of particles and three flow regimes. It is seen that the variance can be expressed in terms of the mean value of the bubble size distribution according to:

$$\sigma^2 = 4.1 \times 10^3 (\bar{d}_n)^{2.0} \tag{18}$$

This relationship indicates that a small mean bubble size is associated with a small variance, which characterizes the dispersed bubble flow. A large mean bubble size can be associated with a large variance, which characterizes the coalesced bubble flow as well as slug flow.

As indicated earlier, all the bubble property distributions presented so far in this study are based on the frequency of the bubbles. As also indicated, large-size bubbles do not possess a spherical geometry. To compare the bubble size, however, a bubble volume distribution function, $F(d)$, is introduced, which assumes a spherical geometry of the bubble:

$$F(d) = \frac{d^3 r(d)}{\int_0^\infty d^3 r(d) dd} \tag{19}$$

Table 1 shows the calculated values of $\bar{d}_v$, the mean bubble size based on the distribution of Eq. 19. It is seen that in general $\bar{d}_v$ is higher than $\bar{d}_n$. In particular, $\bar{d}_v$ is considerably higher than $\bar{d}_n$ in the slug flow regime. This is clearly the effect of the large volume of the gas slugs.


## ACKNOWLEDGMENT

We would like to thank the donors of the Petroleum Research Fund, which is administered by the American Chemical Society, for the support of this research.


## NOTATION

$a$ = insulation constant in Eq. 10 (m)
$d$ = in-bed bubble size (m)

$d_{min}$ = minimum detectable bubble size by a probe (m)
$\bar{d}_n$ = mean bubble size based on number frequency of bubbles (m)
$d_r$ = needle diameter in Eq. 10 (m)
$\bar{d}_v$ = mean bubble size based on volume frequency of bubbles (m)
$F(d)$ = volume distribution function, defined by Eq. 19 (1/m)
$g$ = gravitational acceleration (m/s$^2$)
$H_f$ = expanded bed height (m)
$H_o$ = static bed height (m)
$L_p$ = vertical distance between two probes (m)
$l_b$ = chord length of bubble (m)
$\bar{l}_b$ = mean chord length (m)
$p(d,l_b)$ = probability density function, given by Eq. 6 (1/m)
$Q(u_b)$ = bubble rise velocity distribution (s/m)
$R(\xi)$ = dimensionless bubble size distribution based on number frequency of bubbles
$r(d)$ = bubble size distribution based on number frequency of bubbles (1/m)
$t$ = real time (s)
$u_b$ = bubble rise velocity (m/s)
$\bar{u}_b$ = mean bubble rise velocity (m/s)
$u_g$ = superficial gas velocity (m/s)
$u_l$ = superficial liquid velocity (m/s)
$w_i$ = weight coefficient for numerical integration in Eq. 8
$Z(\lambda)$ = dimensionless chord length distribution
$z(l_b)$ = chord length distribution (1/m)

### Greek Letters

$\alpha$ = scale parameter of log-normal distribution in Eq. 12
$\beta$ = shape parameter of log-normal distribution in Eq. 12
$\Delta d_h$ = horizontal distance between two probes (m)
$\Delta t$ = apparent lag time (s)
$\Delta\tau$ = average residence time of a bubble traveling between two probes (s)
$\lambda$ = dimensionless chord length = $l_b/\bar{d}_n$
$\lambda'$ = dimensionless chord length = $l_b/\bar{l}_b$
$\mu$ = mean of log-normal distribution, defined by Eq. 13
$\xi$ = dimensionless bubble size, = $d/\bar{d}_n$
$\xi_m$ = maximum value of $\xi$
$\sigma^2$ = variance of log-normal distribution, given by Eq. 14
$\tau$ = dwell time (s)
$\bar{\tau}$ = average dwell time (s)

## LITERATURE CITED


Adlington, D., and E. Thompson, "Desulphurization in Fixed and Fluidized Bed Catalyst System," *Proc. 3rd. European Symp. Chem. React. Eng.*, 203 Pergamon Press, Oxford (1965).

Bruce, P. N., and L. Revel-Chion, "Bed Porosity in Three-Phase Fluidization," *Powder Technol.*, **10**, 243 (1974).

Buchholz, R., W. Zakrzewski, and K. Schugerl, "Techniques for Determining the Properties of Bubbles in Bubble Columns," *Int. Chem. Eng.*, **21**, 180 (1980).

Darton, R. C., and D. Harrison, "Some Properties of Gas Bubbles in Three-Phase Fluidized Beds," *I. Chem. Eng. Symp. Ser.*, **I**, No. 38, The Inst. Chem. Engrs., London (1974).

Daries, R. M., and G. I. Taylor, "The Mechanics of Large Bubbles Rising Through Extended Liquids and Through Liquids in Tubes," *Proc. Royal Soc.*, London, Ser. A200, 375 (1950).

El-Temtamy, S. A., and N. Epstein, "Rise Velocities of Large Single Two-Dimensional and Three-Dimensional Gas Bubbles in Liquids and in Liquid Fluidized Beds," *Chem. Eng. J.*, **19**, 153 (1980).

Fan, L.-S., K. Muroyama, and S. H. Chern "Hydrodynamic Characteristics of Inverse Fluidization in Liquid-Solid and Gas-Liquid-Solid Systems," *Chem. Eng. J.*, **24**, 143 (1982).

Fan, L.-S., S. H. Chern, and K. Muroyama, "Qualitative Analysis of Solids Mixing in a Gas-Liquid-Solid Fluidized Bed Containing a Binary Mixture of Particles," *AIChE. J.* **30**, (5) 858 (1984).

Henriksen, H. K., and K. Ostergaard, "Characteristics of Large Two-Dimensional Air Bubbles in Liquids and in Three-Phase Fluidized Bed," *Chem. Eng. J.*, **7**, 141 (1974).

Kuestler, J. L., and J. H. Mize, *Optimization Techniques with FORTRAN*, McGraw-Hill, New York (1973).

Lee, J. C., A. J. Sherrard, and P. S. Buckley, "Optimum Particle Size in Three Phase Fluidized Bed Reactors," *Fluidization and Its Applications*, H. Angelino et al., Eds., 407, Cepadues-Editions, Toulouse (1974).

Massimilla, L., A. Solimando, and E. Squillace, "Gas Dispersion in Solid-Liquid Fluidized Beds," *Brit. Chem. Eng.* **6**, 232 (1961).

Matsuura, A., T. Akehata, and T. Shirai, "Delta-Response by Two-Point Measurement—Axial Mixing of Gas-Liquid Cocurrent Downflow Through Packed Beds," *Kagaku Kogaku Ronbunshu*, **2**, 98 (1976).

Ostergaard, K., "On the Growth of Air Bubbles Formed at a Single Orifice in a Water Fluidized Bed," *Chem. Eng. Sci.*, **21**, 470 (1966).

Page, R. E., and D. Harrison, "The Size Distribution of Gas Bubbles Leaving a Three-Phase Fluidized Bed," *Powder Technol.*, **6**, 245 (1972).

Rigby, G. R., G. P. Van Blockland, W. H. Park, and C. E. Capes, "Properties of Bubbles in Three-Phase Fluidized Bed as Measured by an Electroresistivity Probe," *Chem Eng. Sci.*, **25**, 1729 (1970).

Smith, D. N., W. Fuchs, R. J. Lynn, and D. H. Smith, "Bubble Behavior in a Slurry Bubble Column Reactor Model," ACS Nat. Meeting (Mar., 1983).

Tsutsui, T., and T. Miyauchi, "Fluidity of a Fluidized Catalyst Bed and Its Effect on the Behavior of the Bubbles," *Int. Chem. Eng.*, **20**, 386 (1980).

Ueyama, K., and T. Miyauchi, "Determination of Mean Bubble Diameters Based on Observation by a Two-Point Electric Probe," *Kagaku Kogaku Ronbunshu*, **2**, 430 (1976).

Ueyama, K., S. Morooka, K. Koide, H. Kaji and T. Miyauchi, "Behavior of Gas Bubbles in Bubble Columns," *IEC Proc. Des. Dev.*, **19**, 592 (1980).



*Manuscript received December 15, 1983; revision received July 20, and accepted July 23, 1984.*